© 2016. Published by The Company of Biologists Ltd | Journal of Cell Science (2016) 129, 2075-2084 doi:10.1242/jcs.182261

RESEARCH ARTICLE

ESCRT-0 complex modulates *Rbf*-mutant cell survival by regulating Rhomboid endosomal trafficking and EGFR signaling

Zhentao Sheng[1], Lijia Yu[2], Tianyi Zhang[1], Xun Pei[1], Xuan Li[1], Zhihua Zhang[2] and Wei Du[1,*]

ABSTRACT

The Rb tumor suppressor is conserved in *Drosophila*, and its inactivation can lead to cell proliferation or death depending on the specific cellular context. Therefore, identifying genes that affect the survival of Rb-mutant cells can potentially identify novel targets for therapeutic intervention in cancer. From a genetic screen in *Drosophila*, we identified synthetic lethal interactions between mutations of fly *Rb* (*rbf*) and the ESCRT-0 components *stam* and *hrs*. We show that inactivation of ESCRT-0 sensitizes *rbf*-mutant cells to undergo apoptosis through inhibition of EGFR signaling and accumulation of Hid protein. Mutation of *stam* inhibits EGFR signaling upstream of secreted Spi and downstream of *Rhomboid* expression, and causes Rhomboid protein to accumulate in the abnormal endosomes labeled with both the early and late endosomal markers Rab5 and Rab7. These results reveal that ESCRT-0 mutants inhibit EGFR signaling by disrupting Rhomboid endosomal trafficking in the ligand-producing cells. Because ESCRT-0 also plays crucial roles in EGFR downregulation after ligand binding, this study provides new insights into how loss of ESCRT-0 function can either increase or decrease EGFR signaling.

KEY WORDS: Rhomboid, Stam, Hrs, EGFR signaling, Rbf, Apoptosis

INTRODUCTION

The retinoblastoma tumor suppressor (Rb) is a member of the Rb family and is often inactivated in cancers. This family of proteins functions by binding to a large number of cellular proteins, particularly the E2F family of transcription factors (Morris and Dyson, 2001). There are three subgroups of E2F proteins in mammalian cells: the activating E2F1-3, the repressive E2F4-5 and Rb-independent E2F6-8 (Attwooll et al., 2004; Trimarchi and Lees, 2002). The Rb and E2F proteins are highly conserved but much simpler in *Drosophila melanogaster* (Du and Pogoriler, 2006; Gordon and Du, 2011a; van den Heuvel and Dyson, 2008). There is only one activating E2F protein (*dE2F1*), one repressive E2F protein (*dE2F2*) and two Rb-family proteins (RBF and RBF2) in flies. RBF, which interacts with both dE2F1 and dE2F2, functions like the mammalian Rb protein and regulates cell proliferation, differentiation and apoptosis in *Drosophila* (Du, 2000; Moon et al., 2005; Sukhanova et al., 2011; Tanaka-Matakatsu et al., 2009). By contrast, RBF2, which interacts with dE2F2 but not dE2F1, does not cause obvious defects in cell proliferation, apoptosis or differentiation (Stevaux et al., 2005). The much simpler and yet highly conserved Rb and E2F pathway between *Drosophila* and mammalian systems prompted us to take advantage of the fly system to study this pathway.

The *Drosophila* developing eye provides a model system to identify genes that modulate the proliferation, differentiation or apoptosis of *rbf*-inactivated cells (Gordon et al., 2013; Li et al., 2010; Steele et al., 2009; Tanaka-Matakatsu et al., 2009; Zhang et al., 2014). Photoreceptor differentiation in the developing eye initiates in the morphogenetic furrow (Treisman, 2013). Anterior to the morphogenetic furrow, cells are undifferentiated and asynchronously proliferating. Expression of Ato, which is induced by retinal determination factors and bHLH protein Daughterless just anterior to the morphogenetic furrow (Tanaka-Matakatsu and Du, 2008; Tanaka-Matakatsu et al., 2014, 2015; Zhang et al., 2006), is progressively restricted to small clusters and eventually to the individual R8 precursors within the morphogenetic furrow (Sun et al., 1998). The R8 precursors express the membrane protease Rhomboid (Rho) and release EGFR ligands to activate EGFR signaling, which regulates stepwise retinal differentiation and cell proliferation, and promotes cell survival in posterior eye discs (Baker and Yu, 2001; Dominguez et al., 1998). There are four EGF ligands, representing two different classes – the TGF-α ligands Spitz (Spi), Gurken (Grk) and Keren (Krn), and the neuregulin-like ligand Vein (Vn) (Neuman-Silberberg and Schupbach, 1993; Reich and Shilo, 2002; Rutledge et al., 1992; Schnepp et al., 1996). The main ligand of EGFR in the *Drosophila* eye disc is Spi (Freeman, 1994), which is synthesized as a transmembrane pro-protein (mSpi) (Schweitzer et al., 1995). The post-transcriptional processing of Spi involves the transport of mSpi out of the endoplasmic reticulum (ER) through the chaperone Star (Lee et al., 2001; Tsruya et al., 2002), the palmitoylation of Spi at its N-terminal cysteine residue by the membrane bound O-acyltransferase Rasp (Miura et al., 2006) and the cleavage of Spi by the membrane protease Rhomboid (Urban et al., 2001). In addition to its effect on Spi, Rhomboid can also cleave Star and regulate the level of Spi secretion (Tsruya et al., 2007). In *Drosophila*, *Rhomboid* expression is dynamically regulated, whereas other components of EGFR signaling are ubiquitously expressed. Therefore, the expression pattern of Rhomboid determines the location of the active EGFR ligand release and EGFR signaling activation. Termination of EGFR signaling is regulated at multiple levels, which includes the induction of negative-feedback regulators such as Argos (Aos) and the induction of receptor downregulation involving the Endosomal Sorting Complex Required for Transport (ESCRT) machinery (ESCRT-0 to ESCRT-III) (Katzmann et al., 2002; Williams and Urbe, 2007).

Because the consequences of Rb inactivation, including cell proliferation or cell death, are influenced by additional cell intrinsic factors and extrinsic survival signaling, identification of genes that

[1]Ben May Department for Cancer Research, University of Chicago, 929 E. 57th Street, Chicago, IL 60637, USA. [2]CAS Key Laboratory of Genome Sciences and Information, Beijing Institute of Genomics, Chinese Academy of Sciences, No.1 Beichen West Road, Chaoyang District, Beijing 100101, People's Republic of China.

*Author for correspondence (wei@uchicago.edu)

Received 21 October 2015; Accepted 31 March 2016

Journal of Cell Science (2016) 129, 2075-2084 doi:10.1242/jcs.182261

modulate the proliferation or apoptosis of Rb-inactivated cells *in vivo* will provide new insights into the regulatory mechanisms and potentially identify novel targets for cancer intervention (Gordon and Du, 2011b). Interestingly, inactivation of RBF in the *Drosophila* developing eye causes increased apoptosis mostly in the morphogenetic furrow area (Du, 2000), suggesting the presence of regulatory pathways that affect cell death or survival induced by Rb inactivation. In this manuscript, we characterize several mutants that inactivate ESCRT-0 and that induce cell death in synergy with Rb inactivation.

RESULTS

Mutations of ESCRT-0 components *stam* and *hrs* promote apoptosis in *rbf*-mutant clones

From genetic screening on chromosome 2L to identify genes that are important for the survival of *rbf*-null cells, we isolated three mutations *19*, *4-19-3* and *5-14-3*. Although significant amounts of tissue were observed in *rbf*, *19*, *4-19-3* or *5-14-3* single-mutant clones in adult fly eyes (Fig. 1A–C,E; Fig. S1E, white patches), combining *rbf* mutation with any of these novel alleles showed little double-mutant tissue (Fig. 1D,F; Fig. S1F, white patches). These observations suggest that these mutations promote the elimination of *rbf*-mutant cells during eye development.

To directly test if the observed loss of double-mutant clones in adult eyes correlates with increased apoptosis in developing eye discs, 3rd-instar eye discs from single- or double-mutant clones were stained with an antibody against activated Caspase-3. As shown previously, *rbf*-mutant cells (GFP-negative clones) exhibited increased apoptosis near the morphogenetic furrow with little apoptosis detected in *rbf* clones posterior to the morphogenetic furrow (Fig. 1G, yellow arrow). In addition, single-mutant clones of *19* (Fig. 1H,H′), *4-19-3* (Fig. 1J,J′) or *5-14-3* (Fig. S2D,D′) showed very low levels of Caspase-3 staining. However, significantly increased Caspase-3 staining in posterior eye discs was observed in *rbf 19* (Fig. 1I,I′), *rbf 4-19-3* (Fig. 1K,K′) and *rbf 5-14-3* (Fig. S2E,E′) double-mutant clones (Fig. 1Q; Fig. S2F; $P<0.0005$ between the double-mutant clones and each of the corresponding single-mutant clones, Student's *t*-test). These results suggest that the *19*, *4-19-3* and *5-14-3* mutations induce greater levels of cell death in synergy with *rbf* mutation (hereafter referred to as synergistic cell death) in posterior eye discs, which is correlated with loss of the double-mutant tissue in adult eyes. To further determine whether the synergistic apoptosis observed is limited to the developing eye discs, we further characterized the apoptosis of the single- and double-mutant clones in developing wing discs. Synergistic cell death was also observed in the *rbf 19*, *rbf 5-14-3* and *rbf 4-19-3* double-mutant clones (Fig. 1L–R; Fig. S2J–L; $P<0.0005$ between the double-mutant clones, and each of the corresponding single-mutant clones, Student's *t*-test). Therefore, these mutations promote the apoptosis of *rbf*-mutant cells in multiple tissues.

Mutations *4-19-3* and *5-14-3* were found to be in the same complementation group, whereas mutation *19* was distinct. Recombination and deficiency mapping showed that the mutations responsible for the phenotypes described above in *4-19-3* and *5-14-3* mutants, and those in the *19* mutant were mapped to genomic regions 23A and 32B1–32B4, respectively. Whole-genome sequencing of the *4-19-3* and *19* mutants, and of the *FRT40* control, was performed to identify the specific gene mutations that caused the observed phenotypes. A single G to A mutation in *hepatocyte growth factor-regulated tyrosine kinase substrate* (*Hrs*) was found in *4-19-3*, which caused a Glu264 to Lys substitution in the ubiquitin-binding domain, which is highly conserved and important to mediate the interaction between Hrs and ubiquitylated cargo (Lloyd et al., 2002). A single T to A mutation in *Signal Transducing Adaptor Molecule* (*Stam*) was found in *19*, which caused an amino acid change from Trp269 to Arg in the conserved Src3 homology (SH3) domain of the Stam protein.

Hrs and Stam interact with each other to form the ESCRT-0 complex, which plays important roles in sorting ubiquitylated cargo in endosomes (Williams and Urbe, 2007). To further demonstrate that mutations *19* and *4-19-3* are alleles of *stam* and *hrs*, respectively, we obtained previously generated *stam* and *hrs* alleles. Both $stam^{3297}$ and $stam^{2896}$ (Chanut-Delalande et al., 2010) failed to complement the *19* mutation. In addition, $stam^{3297}$ mutation also induced synergistic cell death with *rbf* mutation (Fig. S2A–C,F–I,L) and caused the loss of double-mutant tissue in adult eyes (Fig. S1A–D). Similarly, both $hrs^{4\text{-}19\text{-}3}$ and $hrs^{5\text{-}14\text{-}3}$ failed to complement the hrs^{D28} null allele (Lloyd et al., 2002). In addition, hrs^{D28} mutation also induced synergistic cell death with *rbf* mutation (Fig. S2L–O). Furthermore, eye-specific knockdown of *Rbf* and *Stam*, or *Rbf* and *Hrs* using RNA interference (RNAi) constructs dramatically reduced the size of adult eyes, whereas RNAi against each of the single genes only exhibited moderate effects (Fig. S1G–L). Taken together, these results demonstrate that inactivation of Hrs and Stam promotes the apoptosis of *rbf*-mutant cells and causes the loss of double-mutant cells in adult tissues.

dE2F1 activity and increased Hid levels contribute to synergetic cell death in *rbf* and *stam* double-mutant tissues

In *Drosophila* eye discs, cell death in *rbf*-mutant tissue is observed near the morphogenetic furrow, which requires dE2F1 activity and is mediated by increased *Hid* expression (Du, 2000; Li et al., 2010; Moon et al., 2005; Tanaka-Matakatsu et al., 2009; Zhang et al., 2014). We examined the effects of *rbf* and *stam* on the levels of Hid protein. Increased levels of Hid protein were detected in *rbf*-mutant clones near the morphogenetic furrow but not in the posterior (Fig. 2A,A′). Although mutation of *stam* alone did not substantially affect Hid protein levels in eye discs (Fig. 2B,B′), substantially increased Hid protein levels were observed in *rbf* $stam^{19}$ double-mutant clones, both near to the morphogenetic furrow and in the posterior eye disc (Fig. 2C,C′). The increased Hid protein in *rbf stam* double-mutant clones in the posterior eye discs correlated with the observed synergistic cell death there (Fig. 1G–I), suggesting that the increase of Hid protein contributes to the cell death. To directly test this possibility, we generated the *rbf stam* double-mutant clones in the hid^{138} mutant background (Tanaka-Matakatsu et al., 2009). hid^{138} mutation completely blocked cell death in *rbf stam* double-mutant clones (Fig. 2D–E′,G; $P<0.0001$, Student's *t*-test).

We further determined whether the observed synergistic cell death in *rbf stam* double-mutant clones requires deregulated dE2F1 activity. We examined the level of cell death in the $de2f1^{i2}$/$de2f1^{729}$ background. $de2f1^{i2}$ encodes a dE2F1 protein with a deletion of the transactivation domain and $de2f1^{729}$ is a P-element insertion mutant that behaves in a manner similar to that of the null (Duronio et al., 1995; Royzman et al., 1997). $de2f1^{i2}$/$de2f1^{729}$ mutants are viable and can rescue the lethality of *rbf*-null mutants (Du, 2000). Significantly reduced cell death was observed in *rbf stam* double-mutant clones in the $de2f1^{i2}$/$de2f1^{729}$ background (Fig. 2D–G, $P<0.0001$, Student's *t*-test). Therefore, deregulated dE2F1 transcriptional activity contributes to the synergistic cell death of *rbf stam* double-mutant cells. Taken together, these results indicate that dE2F1 activity and increased Hid protein level in *rbf stam* double-mutant clones both contribute to the observed synergistic cell death.

Journal of Cell Science

Journal of Cell Science (2016) 129, 2075-2084 doi:10.1242/jcs.182261

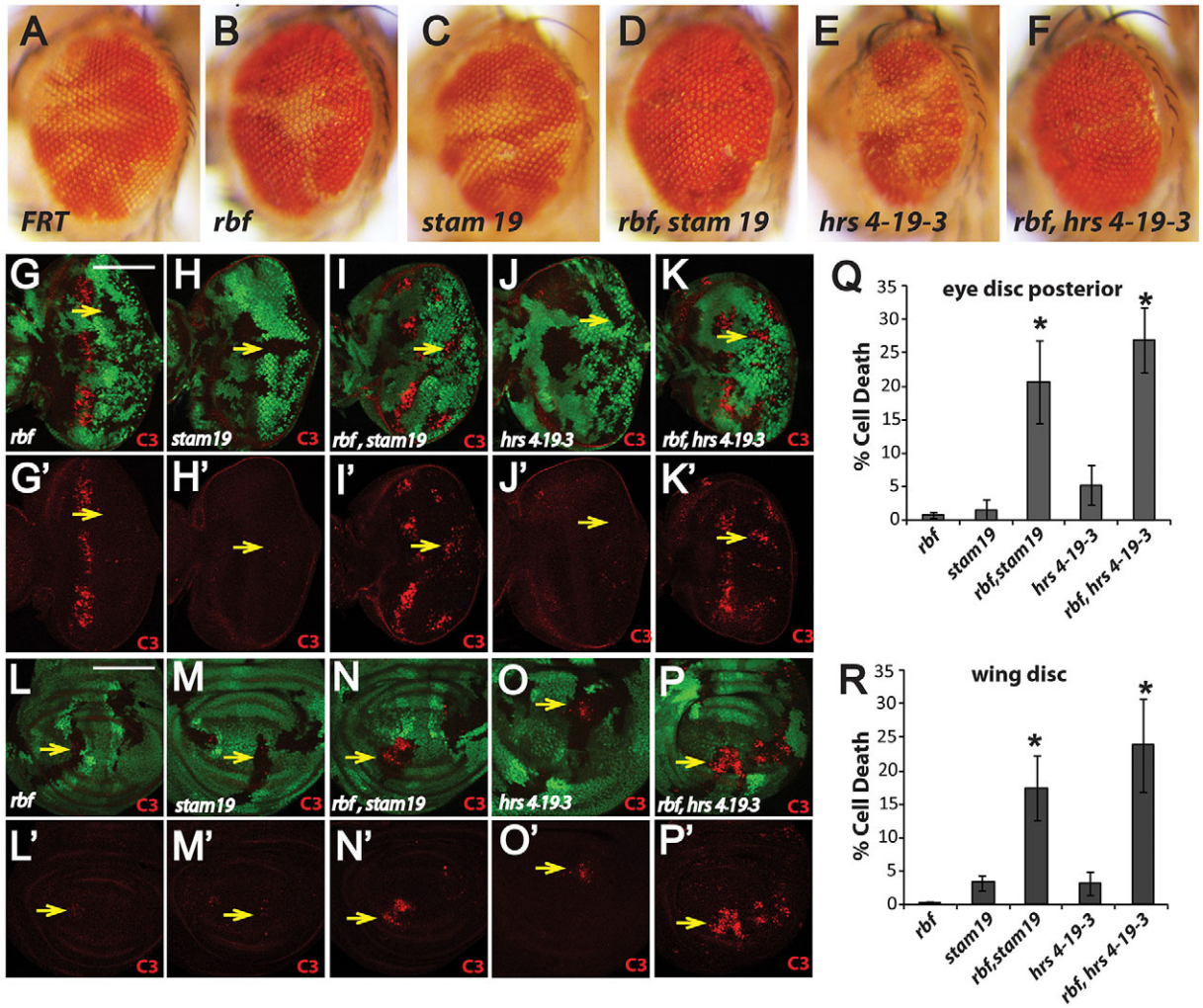

Fig. 1. Mutation of *stam* or *hrs* induces cell death in synergy with *rbf* mutation and promotes the elimination of double-mutant clones in adult eyes. (A–F) Representative pictures of adult eyes with clones of wild-type control (A). (B–F) *rbf*, *stam* and *hrs* single- or double-mutant clones are shown. Mutant clones are marked by lack of red pigment. (G–R) Levels of apoptosis in 3rd instar eye discs (G–K′) or wing discs (L–P′) with *rbf*, *stam* or *hrs* single- or double-mutant clones are shown. Mutant clones are marked by lack of GFP, and an antibody to detect cleaved Caspase-3 (C3) was used to detect apoptosis. Yellow arrows point to mutant clones. The level of apoptosis in mutant clones located in the posterior of eye discs and wing discs was quantified, shown in Q and R respectively. Data are mean±s.d. The number of discs quantified for each genotype was: *rbf*, n=7; $stam^{19}$, n=6; *rbf* $stam^{19}$, n=8; $hrs^{4\text{-}19\text{-}3}$, n=7; *rbf* $hrs^{4\text{-}19\text{-}3}$, n=6. Similar results were observed in three independent experiments. Asterisks indicate a statistically significant difference (P<0.0001, Student's t-test) between double- and single-mutant clones, and the white scale bars indicate 100 µm. In this and all the subsequent figures, eye discs are orientated dorsal up and posterior to the right; different genotype mutant clones are indicated. The complete genotypes of the flies analyzed are detailed in Table S1.

stam and *hrs* mutations impair EGFR signaling

EGFR signaling, which is active in the posterior eye disc, plays important roles in inhibiting apoptosis, at least in part, through MAPK-mediated phosphorylation and degradation of Hid protein (Baker and Yu, 2001; Bergmann et al., 1998). Mutations of ESCRT-0 components have been shown to either increase or decrease EGFR signaling in different settings (Chanut-Delalande et al., 2010; Lloyd et al., 2002; Miura et al., 2008). To determine whether mutation of *stam* or *hrs* affects EGFR signaling in our system, we used *aos–lacZ* reporter to determine the transcription of *argos*, a negative regulator as well as target of EGFR signaling in *Drosophila*. Although expression of the *aos–lacZ* reporter was not substantially affected in *rbf* single-mutant clones (Fig. 3A,A′), substantially reduced *aos–lacZ* reporter expression was observed in *stam* or *hrs* single-mutant clones, as well as in *rbf stam* or *rbf hrs* double-mutant clones (Fig. 3B–E′; Fig. S3A–D). To further confirm that ESCRT-0 loss reduces EGFR signaling, we examined the effect of *stam* mutations on the level of phosphorylated ERK (dpERK; also known as Rolled) (Gabay et al., 1997). Significantly decreased dpERK staining in the posterior of eye discs was observed in the $stam^{19}$ as well as $stam^{3297}$ single-mutant clones (Fig. 3G,G′; Fig. S3E, yellow arrows). The *rbf stam* double-mutant clones showed a similar reduction in dpERK staining, whereas mutation of *rbf* did not significantly affect dpERK staining in posterior eye discs (Fig. 3F–H; Fig. S3F, yellow arrows). Furthermore, the previously characterized hrs^{D28} null mutant, which exhibited increased EGFR signaling in the embryos, also showed reduced dpERK levels in posterior eye discs (Fig. S3G). Therefore, mutation of ESCRT-0 complex components reduced both the EGFR-signaling-mediated MAPK activation and its transcription output in eye discs. It should be pointed out that some mutant cells at the clone border exhibited high dpERK levels (Fig. 3G–H′; Fig. S3E,G), suggesting that the inhibition of EGFR signaling through mutations of *stam* or *hrs* might not be completely cell autonomous.

Journal of Cell Science (2016) 129, 2075-2084 doi:10.1242/jcs.182261

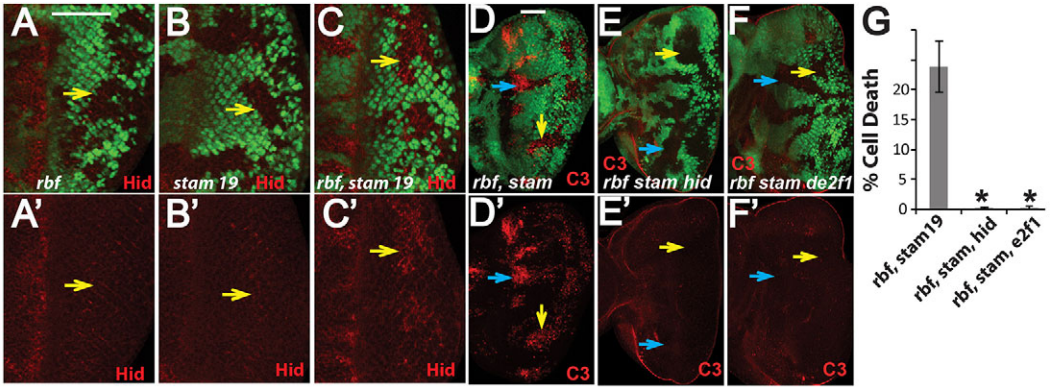

Fig. 2. Synergistic cell death of *rbf stam* double-mutant clones depends on Hid and dE2F1 activity. (A–C′) Hid protein levels in *rbf* and *stam* single- and double-mutant clones were determined by staining with an antibody against Hid. Similar results were observed in different eye discs for each genotype. Mutant clones are marked by lack of GFP; yellow arrows point to mutant clones in the posterior of eye discs. (D–F′) Mutation of *hid* or *de2f1* blocks synergistic apoptosis in *rbf stam* double-mutant clones. Blue and yellow arrows point to mutant clones in the morphogenetic furrow and posterior of eye discs, respectively. The levels of apoptosis in mutant clones located in the posterior of eye discs were quantified, and the means±s.d. are shown in G. The number of discs quantified for each genotype was: *rbf stam*^{19}, n=6; *rbf stam*^{19} *hid*^{138}, n=7; *rbf stam*^{19} *de2f1*, n=6. Results were repeated in three independent experiments. Asterisks indicates a statistically significant difference (P<0.0001, Student's t-test) between triple- and double-mutant clones. The complete genotypes of the flies analyzed are detailed in Table S1. Scale bars: 50 µm.

Because the R8 photoreceptor, the first photoreceptor neuron identified, is the main source of EGFR ligand for the recruitment of additional photoreceptors in developing eye discs, we further characterized the effect of *stam* or *hrs* mutations on photoreceptor differentiation. We found that flies possessing *stam*^{19}, the *hrs*-null mutation *hrs*^{D28} or the *rbf hrs*^{D28} double mutation did not exhibit changes in R8 differentiation, as shown by the normal onset of the R8 marker Senseless (Sens) (Fig. S4A,C,E). These results are consistent with the previous report that *hrs* mutation does not affect R8 differentiation (Miura et al., 2008). In contrast, although *stam*^{19} only slightly delayed additional photoreceptor differentiation, *hrs*^{D28} single and *rbf hrs*^{D28} double mutants exhibited a more substantial delay in photoreceptor differentiation (Fig. S4B,D,F). Because EGFR signaling is required for the differentiation of all photoreceptor cells except R8, these observations suggest that the *hrs* and *stam* mutations decrease, but do not completely block, EGFR signaling and that the reduced EGFR signaling leads to delayed recruitment of additional photoreceptors after R8 differentiation.

We further characterized the effect of *stam* mutation on EGFR signaling activity in wing discs. In wild-type late 3rd instar wing discs, *aos–lacZ* expression was observed in cells adjacent to the wing margin and in the L3, L4 and L5 primordia (Fig. 3I). Mutation of *stam* substantially inhibited *aos–lacZ* levels in cells adjacent to the wing margin area (Fig. 3J,J′, blue arrows) and in L3 primordia (Fig. 3J–K, yellow arrows). By contrast, substantial levels of *aos–lacZ* in L4 primordia were still expressed in *stam*-mutant clones (Fig. 3J,J′, white arrows). The neuregulin-like EGFR ligand Vein plays important roles during wing development (Schnepp et al., 1996). Because Argos expression in the L4 primordia (but not in other regions) of 3rd instar wing discs is significantly decreased in *vn*^{1} mutants (Wessells et al., 1999), Vein is likely to play an important role in the activation of EGFR signaling in L4 primordia, whereas Spi is likely to play a major role in EGFR signaling

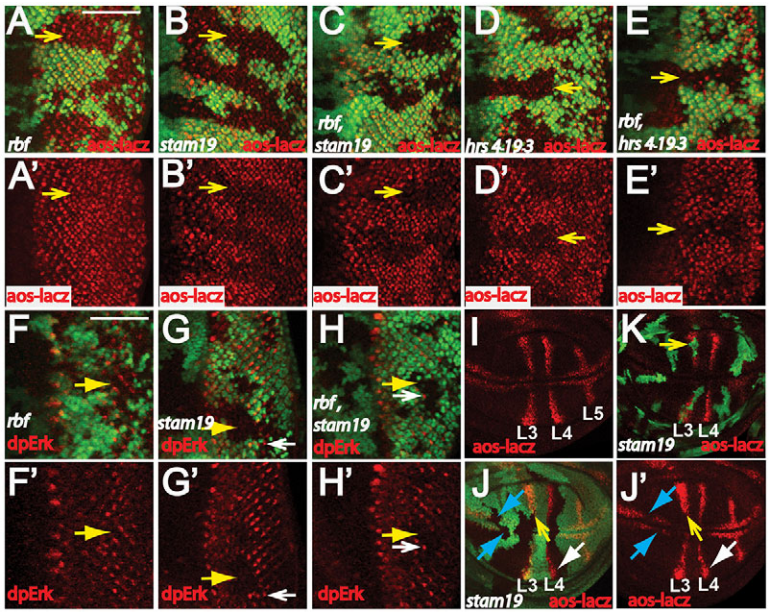

Fig. 3. *stam* and *hrs* mutations decrease activation of EGFR signaling in the posterior of eye discs and wing discs. (A–E′) The effects of *rbf*, *stam* and *hrs* single or double mutants on the levels of the EGFR-signaling target *aos–lacZ* in the posterior of eye discs are shown. (F–H′) The effects of *rbf* and *stam* single- or double-mutant clones on dpERK levels in posterior eye discs are shown. Mutant clones are marked by the lack of GFP, and yellow arrows point to eye disc mutant clones in the posterior. White arrows in G–H′ point to some mutant cells adjacent to wild-type tissue that has high dpERK levels. Similar results were observed for each genotype. (I–K) *stam* mutation significantly decreases EGFR signaling in L3 primordia and near the wing margin area, but only weakly affects EGFR signaling in the L4 primordia. (I) Wild-type pattern of EGFR signaling in late 3rd instar wing discs is shown by the *aos–lacZ* reporter. *aos-lacZ* expression was observed in the wing margin area and in the L3, L4 and L5 primordia. (J,J′) *stam*-mutant clones are marked by the lack of GFP. (K) *stam* MARCM clones are marked by GFP expression. Mutation of *stam* significantly decreases *aos–lacZ* levels in the L3 primordia (yellow arrows in J–K, the strong *aos–lacZ* signals in J′ are in GFP-positive wild-type cells) and in the wing margin area (blue arrows in J). By contrast, substantial levels of the *aos–lacZ* reporter in L4 primordia were still expressed in *stam*-mutant clones (J,J′, white arrow). The complete genotypes of the flies analyzed are detailed in Table S1. Scale bars: 50 µm.

Journal of Cell Science (2016) 129, 2075-2084 doi:10.1242/jcs.182261

activation in most other regions. Therefore, these results support the possibility that *stam* mutation preferentially reduces Spi- but not Vein-induced EGFR signaling activation. Because MAPK activity plays a crucial role in regulating Hid-mediated cell death (Bergmann et al., 1998), these results suggest that decreased EGFR–MAPK signaling in mutant clones of ESCRT-0 components contributes to the synergistic cell death observed with *rbf* mutation.

Mutation of *stam* blocks EGFR signaling upstream of EGFR activation and downstream of Rhomboid expression

In developing eye discs, EGFR signaling activation is mediated by the membrane-tethered ligands (such as Spi) that require processing by the membrane protease Rhomboid, which is expressed in the developing photoreceptors. To determine whether decreased EGFR–MAPK signaling mediates synergistic cell death of *rbf stam* double mutants, we used the Mosaic Analysis with a Repressible Cell Marker (MARCM) system to express Rhomboid, secreted Spi, activated EGFR or activated Ras (Ras^{V12}) in double-mutant clones. *rbf stam* double-mutant MARCM clones were positively labeled with GFP, and they showed considerable levels of Caspase-3 staining (Fig. 4A,A′). Expression of Ras^{V12} significantly decreased the Caspase-3 staining in *rbf stam* double-mutant clones (Fig. 4B,B′,H; $P<0.0001$, Student's *t*-test). Similarly, expression of a constitutively activated form of EGFR ($EGFR^{CA}$) or secreted Spi in the double-mutant clones of *rbf* $stam^{19}$ also significantly decreased Caspase-3 staining (Fig. 4C–D′,H, $P<0.0001$, Student's *t*-test). In contrast, Rhomboid expression failed to decrease Caspase-3 staining in *rbf* $stam^{19}$ double-mutant clones (Fig. 4G–H, $P=0.9$) even though Rhomboid expression blocked cell death in *rbf* single-mutant clones near the morphogenetic furrow (Fig. 4E–F′). These results suggest that *stam* mutation blocks EGFR signaling at a step that is upstream of secreted Spi and activated EGFR receptor but downstream of Rhomboid expression.

We further characterized the effect of *stam* mutation on Rhomboid- or $EGFR^{CA}$-induced *aos–lacZ* and MAPK activation. Rhomboid expression in wild-type eye discs induced precocious *aos–lacZ* expression and dpERK staining anterior to the morphogenetic furrow (Fig. 5A–A″,C–C″). In contrast, Rhomboid expression in *stam*-mutant clones failed to induce precocious *aos–lacZ* or dpERK staining anterior to the morphogenetic furrow (Fig. 5B–B″,D–D″). In addition, the *aos–lacZ* and dpERK levels in posterior eye discs were still reduced in *stam*-mutant clones even with Rhomboid expression (Fig. 5B″,D″), which is similar to that of the *stam*-mutant clones (Fig. 3B,G). Therefore *stam* mutation blocks Rhomboid-induced EGFR signaling activation. In contrast, *stam* mutation did not affect $EGFR^{CA}$-induced *aos–lacZ* or dpERK levels in either the anterior or posterior of eye discs (Fig. 5E–H″). Furthermore, null alleles of the ESCRT-0 mutants $stam^{2896}$ and hrs^{D28} did not affect $EGFR^{CA}$-induced *aos–lacZ* levels (Fig. S3H–J). These results show that *stam* mutation inhibits EGFR signaling upstream of EGFR activation and downstream of Rhomboid expression.

Because Rhomboid is required for Spi processing, we tested the effect of *stam* mutation on secreted Spi (sSpi) (Schweitzer et al., 1995) using the MARCM approach. Expression of sSpi strongly increased *aos–lacZ* levels both in sSpi-expressing clones as well as in cells surrounding the clone, probably owing to the diffusion of the sSpi ligand (Fig. 5I–I″, compare with the background levels pointed by white arrows). It is interesting to note that sSpi induced stronger *aos–lacZ* levels in cells surrounding the clones, probably owing to the induction of receptor downregulation and negative-feedback regulation in the presence of excess levels of sSpi. Importantly, sSpi expression still induced ectopic *aos–lacZ* expression in *stam* clones

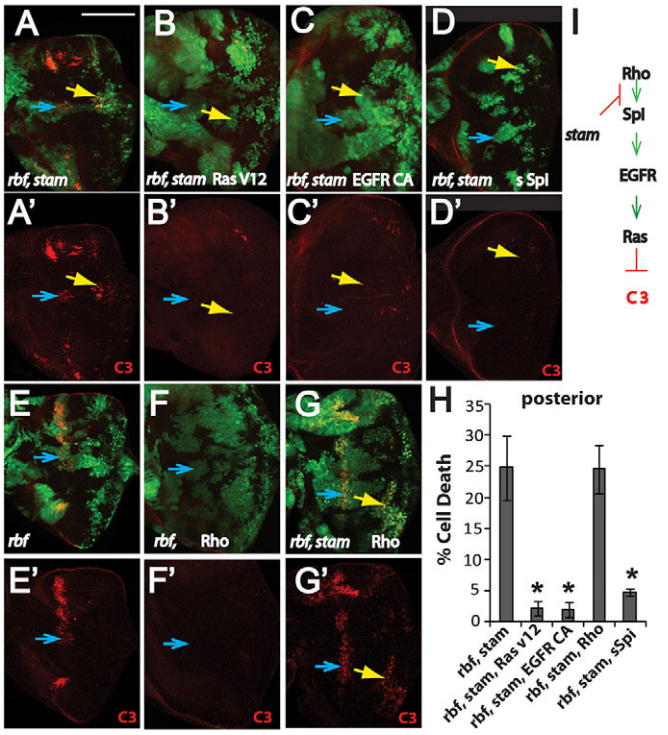

Fig. 4. Synergistic cell death of *rbf stam* double mutants is suppressed by expression of activated Ras, activated EGFR and secreted Spi but not by Rhomboid expression. (A–G′) *rbf stam* (A–D′,G,G′) and *rbf* (E–F′) MARCM clones are marked by GFP expression, and apoptotic cells are identified by Caspase-3 (C3) staining shown in red. Apoptosis in the morphogenetic furrow and posterior are indicated by blue and yellow arrows, respectively. (H) The levels of apoptosis in the indicated genotypes of *rbf stam* double-mutant MARCM clones located in the posterior of eye discs were quantified. The mean±s.d. are shown. The number of discs quantified for each genotype was: *rbf* $stam^{19}$, $n=8$; *rbf* $stam^{19}$ ras^{v12}, $n=6$; *rbf* $stam^{19}$ $EGFR^{CA}$, $n=6$; *rbf* $stam^{1}$ *sSpi*, $n=9$; *rbf* $stam^{19}$ *rho*, $n=7$. Asterisks indicate statistically significant difference ($P<0.0001$, Student's *t*-test) between triple- and double-mutant clones. Similar results were observed in three independent experiments. (I) A diagram that summarizes where *stam* mutation blocks EGFR signaling activation. The complete genotypes of the flies analyzed are detailed in Table S1. Scale bar: 100 µm.

(Fig. 5J–J″, yellow arrows, compare with the background *aos–lacZ* levels pointed by white arrows), and mutation of *stam* did not significantly affect sSpi-induced *aos–lacZ* levels either within the clone or in cells surrounding the clones (Fig. 5I–J″). These observations indicate that *stam* mutation does not block the release of sSpi or its activation of EGFR signaling. Taken together, our results show that *stam* mutation blocks EGFR signaling downstream of Rhomboid expression and upstream of secreted Spi.

Mutation of *stam* causes accumulation of Rhomboid in abnormal endosomal compartments

Rhomboid has been shown to localize to the endosomes (Tsruya et al., 2007). In wild-type eye discs, Rhomboid is expressed in the posterior and can be detected by an antibody against Rhomboid as endosome-localized small spots (Sturtevant et al., 1996; Sukhanova et al., 2011) (see also Fig. 6F,G). Interestingly, larger and brighter Rhomboid spots were observed in *stam*- or *hrs*-mutant clones (Fig. 6B,C). The effect of *stam* or *hrs* mutation on Rhomboid is not due to alteration of expression because levels of the enhancer trap *Rhomboid–lacZ* were unaffected (Fig. 6D,E). Because ESCRT-0 affects endosomal trafficking, these observations raised the

Journal of Cell Science (2016) 129, 2075-2084 doi:10.1242/jcs.182261

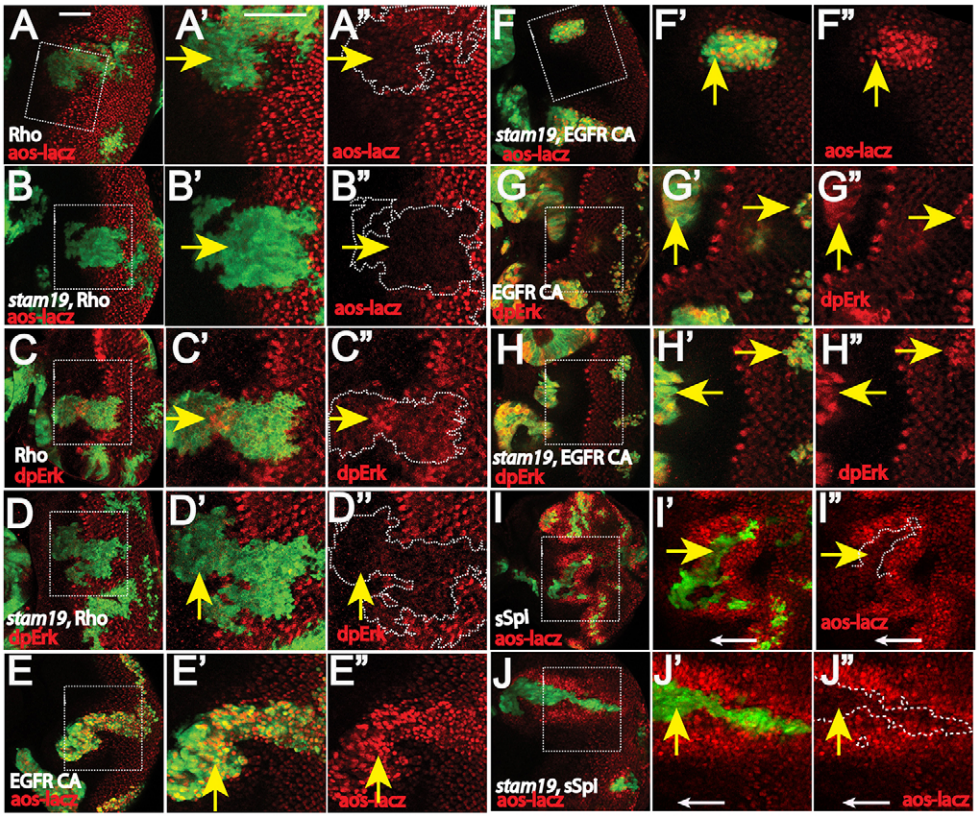

Fig. 5. Effect of *stam* mutation on EGFR signaling induced by Rhomboid, secreted Spi or activated EGFR. Rhomboid (Rho) expression in wild-type discs (A–A″ and C–C″) induces precocious *aos–lacZ* expression (A–A″) and dpERK (C–C″) anterior to the morphogenetic furrow. In contrast, Rhomboid expression in *stam* MARCM clones (marked by GFP) failed to induce precocious *aos–lacZ* (B–B″) or dpERK levels (D–D″). By contrast, expression of activated EGFR induces precocious *aos–lacZ* (E–F″) and dpERK levels (G–H″) in both the wild-type background (E–E″,G–G″) and the *stam* MARCM clones (F–F″,H–H″). (I–J″) Expression of secreted Spi in the wild-type background (I–I″) and in *stam* MARCM clones (J–J″). sSpi expression induces substantial precocious *aos–lacZ* expression both within the sSpi-expressing cells (marked by GFP) and in cells adjacent to the sSpi-expressing cells in either the wild-type background (I–I″) or in *stam* MARCM clones (J–J″). White arrows in I′–I″ and J′–J″ point to background *aos–lacZ* levels in anterior eye discs. Multiple discs were examined and representative results for each genotype are shown. The complete genotypes of the flies analyzed are detailed in Table S1. Yellow arrows point to Rho, sSpi or $EGFR^{CA}$ MARCM clones. Panels labeled ′ and ″ correspond to the zoomed in image of the boxed areas. The white dashed lines outline the MARCM clones. Scale bars: 50 µm.

possibility that *hrs* and *stam* mutation interferes with normal Rhomboid endosomal transport. Consistent with this possibility, the larger and brighter Rhomboid spots were also observed in clones of ESCRT-I, ESCRT-II and ESCRT-III mutants (Fig. S4G–I′). In addition, the ESCRT-I–ESCRT-III mutants also exhibited substantially decreased EGFR signaling, as shown by reduced *aos–lacZ* levels (Fig. S4J–L′). These observations suggest that inactivation of any of the ESCRT complexes blocks normal Rhomboid endosomal trafficking and inhibits EGFR signaling. Consistent with this, RNAi of ESCRT-I components also decreases dpERK levels, although ESCRT-I inactivation inhibits dpERK levels downstream of EGFR activation (Miura et al., 2008). It is possible that although all the ESCRT complexes can block Rhomboid trafficking and inhibit EGFR signaling, ESCRT-I and ESCRT-II can also block EGFR signaling activation downstream of receptor activation.

We used the early-endosome marker Rab5 and the late-endosome marker Rab7 to further characterize the effect of *stam* mutation on Rhomboid localization. Previous reports have shown that overexpressed Rhomboid is localized in the Rab4, Rab14 and Rab7 endosomes but rarely in the Rab5 endosomes (Tsruya et al., 2007; Yogev et al., 2010). Consistent with this, we found that endogenous Rhomboid protein rarely colocalized with Rab5 but partially colocalized with Rab7 (Fig. 6F–G″). *hrs* mutation has been shown to cause enlarged endosomes and block multivesicular body (MVB) formation (Lloyd et al., 2002). Interestingly, in *stam*-mutant clones, Rhomboid accumulated in enlarged endosomes that often had the early-endosome marker Rab5 and late-endosome marker Rab7 (Fig. 6H–I″). Therefore, mutation of ESCRT-0 perturbs the endosome compartment and traps Rhomboid in the abnormal endosomes.

The localization of Rhomboid to the abnormal endosomes in *stam*-mutant clones can potentially block EGFR signaling by preventing Rhomboid and Spi from localizing to the same compartment. To test this possibility, we used the Sca–Gal4 driver to express membrane Spi (mSpi) in the developing R8 cells in order to determine colocalization between mSpi and endogenous Rho. Colocalization of mSpi and Rhomboid could be detected both in wild-type cells as well as in *stam*-mutant clones (Fig. 6J, white and yellow arrows). Therefore, *stam* mutation does not prevent Spi and Rhomboid from colocalizing to the same endosomal compartment. It is possible that the abnormal endosomes prevent the colocalized Spi from being trafficked to the location at which it is required to activate EGFR signaling.

DISCUSSION

In this report, we show that inactivation of the ESCRT-0 components *stam* or *hrs* induced synergistic cell death with *rbf*-inactivation by inhibiting EGFR signaling. In addition, *stam* and *hrs* mutants delay photoreceptor differentiation after R8 determination.

Journal of Cell Science (2016) 129, 2075-2084 doi:10.1242/jcs.182261

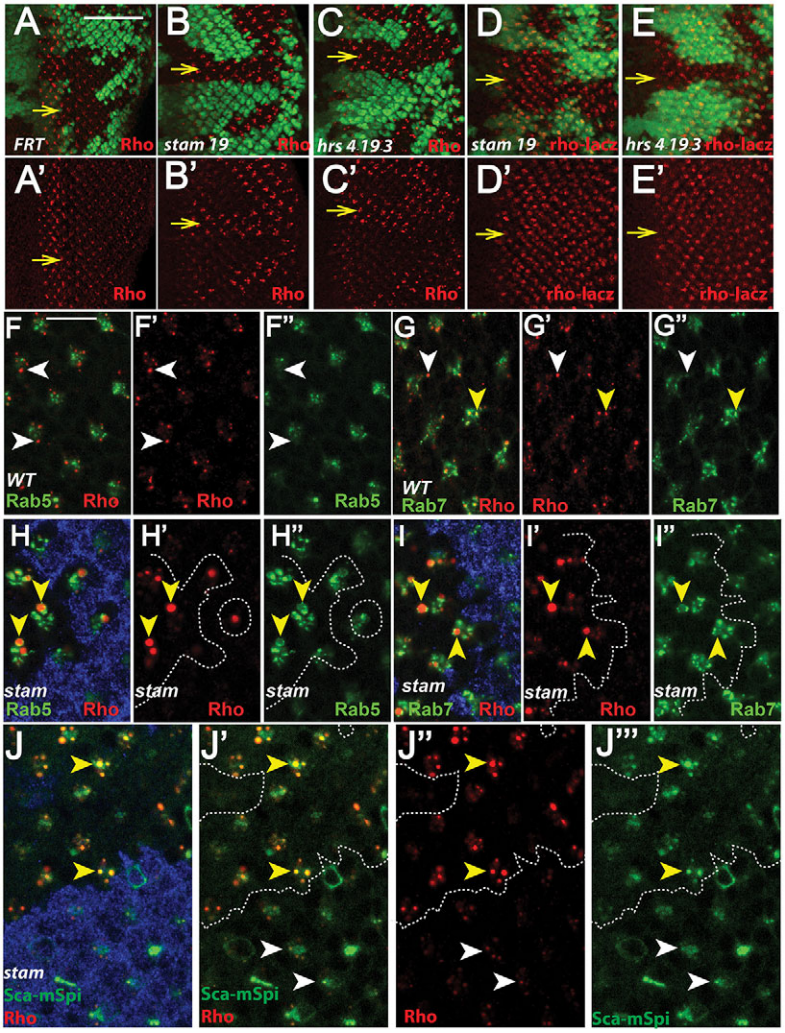

Fig. 6. *stam* and *hrs* mutations cause abnormal localization of Rhomboid in endosomes. (A–E) Effects of *stam* and *hrs* mutations on Rhomboid (Rho) protein levels (A–C′) and on *Rhomboid–lacZ* enhancer trap expression (D–E) are shown. Yellow arrows point to mutant clones, which are marked by the lack of GFP. (F–I″) Colocalization study of Rhomboid with YFP-tagged Rab5 (F–F″ and H–H″) or Rab7 (G–G″ and I–I″) in wild-type (WT) eye discs (F–G″) or eye discs with *stam*-mutant clones (H–I″). White arrowheads point to Rhomboid that did not show colocalization, and yellow arrowheads point to Rhomboid that showed colocalization with Rab5 or Rab7. (J–J‴) Colocalization study of Rhomboid and membrane Spi (mSpi) expressed in R8 cells (using the Sca–Gal4 driver; Sca-mSpi) in a *stam*-mutant clone (indicated by yellow arrowheads) and in adjacent wild-type tissues (indicated by white arrowheads). Multiple discs were examined, and representative results for each genotype are shown. Mutant clones in H–J‴ are marked by the lack of β-galactosidase staining (shown in blue). The complete genotypes of the flies analyzed are detailed in Table S1. Scale bars: 50 µm (A); 10 µm (F). The white dashed lines outline the *stam*-mutant clones.

Because EGFR signaling is required for the differentiation of all the photoreceptors except R8 (Dominguez et al., 1998), it is likely that the reduced EGFR signaling in *stam* and *hrs* mutants also contributes to the delayed photoreceptor differentiation phenotypes. It is worth pointing out that the photoreceptor differentiation delay phenotype of *hrs* or *stam* is reminiscent of that of *rno*, which also inhibits EGFR signaling (Sukhanova et al., 2011). However, because mutation of *rno* blocks EGFR signaling in the nucleus downstream of MAPK activation, *rno* mutation does not inhibit MAPK activity, and *rbf rno* mutation does not result in synergistic cell death (Steele et al., 2009; Sukhanova et al., 2011). The lack of synergistic cell death despite substantial differentiation delay in *rbf rno* double mutants suggests that the synergistic cell death of *rbf stam* cells is likely to be due to reduced MAPK activity in the posterior eye disc rather than to the indirect effect of delayed photoreceptor differentiation. However, because *stam* and *hrs* mutants have been shown to affect the localization of a large number of receptors in different signaling pathways, the possibility that other pathways also contribute to the synergistic cell death of *rbf stam* double mutants cannot be excluded.

Previously, mutations of *axin*, *gig* and *Drosophila Tsc1* (*dTsc1*) have also been reported to induce synergistic cell death with *rbf* (Gordon et al., 2013; Hsieh et al., 2010; Li et al., 2010; Zhang et al., 2014). Interestingly, although synergistic cell death of *rbf stam* double-mutant cells is restricted in posterior eye discs, synergistic cell death in *rbf axin*, *rbf gig* or *rbf dTsc1* double-mutant clones is more prominent in the anterior proliferating region of the eye disc. The distinct patterns of synergistic cell death observed in different double-mutant clones are mediated by different mechanisms. The synergistic cell death in *rbf axin*, *rbf gig* and *rbf dTsc1* double-mutant cells is mediated by excessive cellular stress and increased dE2F1 levels (Gordon et al., 2013; Hsieh et al., 2010; Li et al., 2010; Zhang et al., 2014), whereas synergistic cell death of *rbf stam* or *rbf hrs* mutants in posterior eye discs is mediated by reduced EGFR signaling. In addition, mutation of *groucho*, which causes de-repression of Rhomboid expression and precocious EGFR signaling activation in eye discs (Zhang and Du, 2015), can suppress cell death in *rbf* mutants near the morphogenetic furrow (our unpublished results). The dependency of *rbf*-mutant cell apoptosis in the morphogenetic furrow and posterior eye disc on EGFR signaling suggests that this system can potentially be used to identify additional modulators of EGFR signaling.

Previous reports have shown that mutation of *hrs* enhances EGFR signaling owing to a block in endosomal trafficking that results in EGFR degradation in the developing embryos (Lloyd et al., 2002). By contrast, *stam* and *hrs* mutations have also been shown to inhibit EGFR signaling in eye and wing discs (Chanut-Delalande et al., 2010; Miura et al., 2008), but the mechanism is unknown. Here, we show that *stam* and *hrs* mutations inhibit EGFR signaling by blocking the normal endosomal trafficking of Rhomboid.

Journal of Cell Science (2016) 129, 2075-2084 doi:10.1242/jcs.182261

Furthermore, we show that *stam* mutation leads to the accumulation of Rhomboid in enlarged endosomes that were positive for the early-endosome marker Rab5 and the late-endosome marker Rab7.

A recent report has shown that unprocessed Spi can be observed at the apical surface of the polarized epithelia in the presence of Star, but such Spi is inactive owing to the localization of the receptor in the basal lateral region (Steinhauer et al., 2013). In that report, it is suggested that Spi is endocytosed, cleaved by Rhomboid in endosomes and released to the basal lateral region to activate EGFR signaling (Steinhauer et al., 2013). Alternatively, Spi can potentially enter the Rhomboid-containing endosomes from Golgi and be released to the appropriate location after processing by Rhomboid (Yogev et al., 2010). Because Rhomboid localizes both in the Rab4-type fast recycling endosomes and in the Rab14-positive endosomes that mediate trafficking between Golgi and endosomes (Yogev et al., 2010), it is possible that both mechanisms contribute to the pool of active Spi ligand *in vivo*. This would be consistent with the observation that inactivation of either Rab4 or Rab14 does not result in any discernible phenotype, but inactivation of Rab11 inhibits EGFR signaling in developing eye discs (Yogev et al., 2010). Interestingly, expression of membrane Spi in R8 cells revealed that *stam* mutation does not block colocalization of membrane Spi and Rhomboid (Fig. 6J). It is possible that Spi that is localized in the abnormal endosomes cannot be properly exported in order to activate EGFR signaling, even if it is cleaved by Rhomboid in the same compartment.

In addition to regulating Rhomboid trafficking and active ligand release, which positively regulates EGFR signaling, ESCRT proteins can also negatively regulate EGFR signaling through receptor downregulation after ligand binding (Fischer et al., 2006; Dobrowolski et al., 2012). Indeed, *hrs* mutants have been shown to exhibit decreased receptor downregulation and increased EGFR signaling in embryos (Lloyd et al., 2002). In contrast, our results show that mutation of *stam* or *hrs* decreases EGFR signaling in imaginal discs. Therefore, *stam* and *hrs* mutations can potentially either decrease or increase EGFR signaling, depending on specific tissues or developmental stages. Although the exact mechanism of the differential effects of *stam* and *hrs* mutants on EGFR signaling has not been established, there are a number of possibilities. One is that activation of EGFR signaling by different ligands can potentially contribute to the differential effects of *hrs* mutation on EGFR signaling. There are four different EGFR ligands in flies: Spi, Grk, Vein and Keren. Vein is unique in that it is a secreted soluble EGFR ligand, whereas the others are membrane tethered. Therefore, EGFR activation by Vein is likely to be independent of Rhomboid and Star, and localized expression of Vein contributes to the localized activation of EGFR signaling (Schnepp et al., 1996). Interestingly, although Vein has been shown to play important roles in the induction of EGFR signaling activation in L4 primordia, but not in other regions of 3rd instar wing disc (Wessells et al., 1999), we found that *stam* mutation only weakly decreased *aos–lacZ* upregulation in the L4 primordia but substantially inhibited *aos–lacZ* in other wing disc regions (Fig. 3J). These results are consistent with the possibility that *stam* mutation preferentially reduces Spi- but not Vein-induced EGFR signaling activation. In addition, the membrane tethered EGFR ligands can differ in their dependence on processing by Rhomboid and Star proteins. For example, although Spi is strictly dependent on Rhomboid and/or Star to activate EGFR, Krn can undergo low-level cleavage and activate EGFR independent of Rhomboid and/or Star (Reich and Shilo, 2002). Another possibility is that in some tissues that are not polarized, EGFR signaling can potentially be activated by the unprocessed ligands exported by Star (Steinhauer et al., 2013). In this case, Stam and Hrs mainly regulate EGFR downregulation after ligand binding. Finally, the level of activation of EGFR signaling is likely to be influenced by the specific cellular background, feedback regulation, ligand levels, assay time, etc. For example, it is somewhat unexpected that higher EGFR signaling levels are induced in cells surrounding the sSpi-expressing clones than those in the sSpi-expressing cells (Fig. 5I). Because sSpi can still be palmitoylated, which enhances membrane association and restricts diffusion, sSpi-expressing cells are expected to be exposed to higher concentrations of sSpi ligands than the surrounding cells. It is possible that at the very high concentrations of sSpi, EGFR signaling is no longer limited by the level of sSpi ligand but is limited by the availability of EGFR, which is potentially depleted by the excess sSpi ligand in the overexpressing clones. Therefore, under this specific circumstance, higher levels of sSpi induce lower levels of EGFR signaling activation when assayed several days after sSpi clone induction.

MATERIALS AND METHODS

Drosophila stocks and genetics

Fly stocks used in this study were: $rbf^{15a\Delta}$ (Zhang et al., 2014), hid^{138} (Tanaka-Matakatsu et al., 2009), $de2f1^{i2}$ (Royzman et al., 1997), $de2f1^{rm729}$ (Duronio et al., 1995), $stam^{3297}$, $stam^{2896}$ (Chanut-Delalande et al., 2010), hrs^{D28} (BL54574), *aos–lacZ* (BL2513), *rho–lacZ* (Freeman et al., 1992), UAS–Rho (Zhang and Du, 2015), UAS–sSpi (Miura et al., 2006), UAS–mSpi–GFP (Yogev et al., 2010), UAS–stam RNAi (BL35016), UAS–hrs RNAi (BL28026), UAS–Rbf RNAi (BL36744), UAS–YFP.Rab5 (BL24616), UAS–YFP.Rab7 (BL23270), $UAS–EGFR^{CA}$ (BL9533), $UAS–ras^{v12}$ (BL4847), $Vps28^{D2}$ (BL39624), *Vps22* (BL39631), *Vps32* (BL39623), Sca–gal4(BL6479), Long GMR–Gal4 (BL8121).

Flies were cultured at 25°C on standard cornmeal-yeast-agar medium. Double-mutant clones of *rbf* and *stam* (or *hrs*) were generated in a manner similar to that described previously (Tanaka-Matakatsu et al., 2009; Zhang et al., 2014) except that an RBF genomic rescue construct *RBF-G3* inserted on chromosome 2L was used. This RBF rescue construct completely rescues the viability and fertility of *rbf*-null mutants. The exact genotypes used in this study are detailed in Table S1.

Genetic screen for mutations that modulate the phenotypes of *rbf* mutants

To identify mutations on chromosome 2L that can modulate the phenotypes of *rbf*, ethyl methanesulfonate (EMS) was used to generate mutants, which were then screened, in a manner similar to that described previously (Tanaka-Matakatsu et al., 2009). Isogenized *w*; *p{ry+, neoFRT40A}* males were used for mutagenesis, $rbf^{15a\Delta}$*,w, eyFLP*; *p{ry+, neoFRT40A} p{w+, Ubi-GFP} p{w+, rbf-G3}* and *w, eyFLP*; *p{ry+,neoFRT40A} p{w+, Ubi-GFP}* stocks were used for screening and an *rbf* dependence test. Mutations that gave *rbf*-dependent phenotypes were further mapped with a chromosome 2L deficiency kit from Bloomington, and the precise mutations were identified by whole-genome sequencing.

Whole-genome sequencing and alignment of sequencing reads

Genomic DNA from homozygous mutants of *19*, *4-19-3* and isogenized *FRT40A* controls were prepared and sequenced. The raw reads were filtered with fastx-tools (http://hannonlab.cshl.edu/fastx_toolkit/commandline.html) to remove the low quality reads which 50% bases under the quality score 20. The reads were further trimmed into 80 bp length with quality scores larger than 20. The filtered reads were mapped to FlyBase r5.33 using BWA (version 0.6.1) with no more than three mismatches. The reads that showed unique differences were further analyzed in order to identify mutations.

Mutation detection

The consensus sequences were generated by SAMtools (version 0.1.18) with a quality score of 22 based on the published report (Blumenstiel et al.,

2009). All repeat regions were masked by RepeatMasker. SAMtools and BCFtools were used to call single nucleotide polymorphisms (SNPs), and the maximum read depth for each mutation site was less than 100 (SNPs with super high coverage might be caused by copy number variation). For each pairing of wild-type sample and mutant sample, the mutation site was called twice. First, wild-type was used as reference to identify the mutation sites in the mutant sample. Second, the mutant sample was used as a reference to identify the 'mutation sites' in the wild-type sample. A candidate mutation was retained if it could be found using the above two steps. All mutations were annotated with SnpEff, which reports the non-synonymous mutation sites. Combining the mapping data with these analyses allowed the identification of phenotype-causing mutations in *19* and *4-19-3*.

Immunostaining

Immunostaining was performed at room temperature. Larval imaginal discs were dissected in 1× PBS, fixed with 4% formaldehyde in PBS for 30 min, washed twice with 1× PBS with 0.3% Triton-X100 (PBST), blocked in blocking solution (PBST plus 10% normal goat serum) for 1 h and incubated with primary antibody in blocking solution overnight at 4°C. Primary antibodies were: rabbit anti-activated-Caspase-3 (C3, 1:300 from Cell Signaling, catalog #9661S), rabbit anti-Rhomboid (Rho, 1:500, gift from Dr. Ethan Bier; Sturtevant et al., 1996), rabbit anti-dpErk (1:400, Cell Signaling, catalog #4370S), mouse anti-β-galactosidase (1:100, Developmental Studies Hybridoma Bank, catalog #40-1a) and anti-Hid (1:500, gift from Dr. Don Ryoo; Ryoo et al., 2004). Following incubation with primary antibody, samples were washed three times (10 min each) in PBST, incubated with secondary antibodies from Jackson ImmunoResearch (1:400) for 1 h and washed three times with PBST. Samples were mounted in 70% glycerol with 1,4-diazabicyclo[2.2.2]octane (DABCO) at 12.5 mg/ml. Imaging was performed with the Zeiss Axio observer microscope with ApoTome using the AxioCam CCD camera controlled by Zeiss Axiovision software.

Quantification of cell death levels in developing imaginal discs

Cell death (%) was determined as described previously (Li et al., 2010) by calculating the percentage of the clone area (pixels) that exhibited above background levels of Caspase-3 signal by using the histogram function in Photoshop. The background level of Caspase-3 signal was determined as the level that was equal to or below 99% of the Caspase-3 signal in the wild-type tissues that exhibited no apoptosis. The average and standard deviation of the percentage cell death for a disc of each genotype was then determined and compared for at least six imaginal discs. Two-way Student's *t*-test was used to determine the significance of statistical differences between different genotypes.

Acknowledgements

We would like to thank Drs Jessica Treisman, Ben-Zion Shilo, Matthew Freeman, Marcus Affolter, Ethan Bier and Don Ryoo for providing fly stocks and reagents. We thank the Bloomington Stock Center (National Institutes of Health funded P40OD018537) for providing fly stocks and the Developmental Studies Hybridoma Bank (DSHB; created by the National Institute of Child Health and Human Development of the National Institutes of Health and maintained at The University of Iowa) for providing antibodies. We would also like to thank Dr Gabe Gordon for reading the manuscript and members of the Du lab for many discussions.

Competing interests

The authors declare no competing or financial interests.

Author contributions

Z.S. and W.D. designed the experiments and wrote the manuscript. Z.S. collected data presented in this manuscript. T.Z., Z.S., X.P. and X.L. performed the genetic screen and the genetic mapping studies. L.Y. and Z.Z. performed whole-genome sequencing and mutation identification.

Funding

This work was supported by grants from National Institutes of Health [grant numbers CA149275 and GM074197] to W.D.; and from the National Natural Science Foundation of China [grant number 31271398, 91131012] to Z.Z. Deposited in PMC for release after 12 months.

Data availability

Whole-genome sequencing data for the indicated mutants have been deposited at http://gsa.big.ac.cn with the following accession numbers: *FRT40A* control, CRR006280; *stam* mutation (*19*), CRR006281; *Hrs* mutation (*4-19-3*), CRR006282.

Supplementary information

Supplementary information available online at http://jcs.biologists.org/lookup/suppl/doi:10.1242/jcs.182261/-/DC1

References

Attwooll, C., Lazzerini Denchi, E. and Helin, K. (2004). The E2F family: specific functions and overlapping interests. *EMBO J.* **23**, 4709-4716.

Baker, N. E. and Yu, S.-Y. (2001). The EGF receptor defines domains of cell cycle progression and survival to regulate cell number in the developing Drosophila eye. *Cell* **104**, 699-708.

Bergmann, A., Agapite, J., McCall, K. and Steller, H. (1998). The Drosophila gene hid is a direct molecular target of Ras-dependent survival signaling. *Cell* **95**, 331-341.

Blumenstiel, J. P., Noll, A. C., Griffiths, J. A., Perera, A. G., Walton, K. N., Gilliland, W. D., Hawley, R. S. and Staehling-Hampton, K. (2009). Identification of EMS-induced mutations in Drosophila melanogaster by whole-genome sequencing. *Genetics* **182**, 25-32.

Chanut-Delalande, H., Jung, A. C., Baer, M. M., Lin, L., Payre, F. and Affolter, M. (2010). The Hrs/Stam complex acts as a positive and negative regulator of RTK signaling during Drosophila development. *PLoS ONE* **5**, e10245.

Dobrowolski, R. and De Robertis, E. M. (2012). Endocytic control of growth factor signalling: multivesicular bodies as signalling organelles. *Nat. Rev. Mol. Cell Biol.* **13**, 53-60.

Domínguez, M., Wasserman, J. D. and Freeman, M. (1998). Multiple functions of the EGF receptor in Drosophila eye development. *Curr. Biol.* **8**, 1039-1048.

Du, W. (2000). Suppression of the rbf null mutants by a de2f1 allele that lacks transactivation domain. *Development* **127**, 367-379.

Du, W. and Pogoriler, J. (2006). Retinoblastoma family genes. *Oncogene* **25**, 5190-5200.

Duronio, R. J., O'Farrell, P. H., Xie, J. E., Brook, A. and Dyson, N. (1995). The transcription factor E2F is required for S phase during *Drosophila* embryogenesis. *Genes Dev.* **9**, 1445-1455.

Fischer, J. A., Eun, S. H. and Doolan, B. T. (2006). Endocytosis, endosome trafficking, and the regulation of Drosophila development. *Annu. Rev. Cell Dev. Biol.* **22**, 181-206.

Freeman, M. (1994). The spitz gene is required for photoreceptor determination in the Drosophila eye where it interacts with the EGF receptor. *Mech. Dev.* **48**, 25-33.

Freeman, M., Kimmel, B. E. and Rubin, G. M. (1992). Identifying targets of the rough homeobox gene of Drosophila: evidence that rhomboid functions in eye development. *Development* **116**, 335-346.

Gabay, L., Seger, R. and Shilo, B.-Z. (1997). In situ activation pattern of Drosophila EGF receptor pathway during development. *Science* **277**, 1103-1106.

Gordon, G. M. and Du, W. (2011a). Conserved RB functions in development and tumor suppression. *Protein Cell* **2**, 864-878.

Gordon, G. M. and Du, W. (2011b). Targeting Rb inactivation in cancers by synthetic lethality. *Am. J. Cancer Res.* **1**, 773-786.

Gordon, G. M., Zhang, T., Zhao, J. and Du, W. (2013). Deregulated G1-S control and energy stress contribute to the synthetic-lethal interactions between inactivation of RB and TSC1 or TSC2. *J. Cell Sci.* **126**, 2004-2013.

Hsieh, T.-C., Nicolay, B. N., Frolov, M. V. and Moon, N.-S. (2010). Tuberous sclerosis complex 1 regulates dE2F1 expression during development and cooperates with RBF1 to control proliferation and survival. *PLoS Genet.* **6**, e1001071.

Katzmann, D. J., Odorizzi, G. and Emr, S. D. (2002). Receptor downregulation and multivesicular-body sorting. *Nat. Rev. Mol. Cell Biol.* **3**, 893-905.

Lee, J. R., Urban, S., Garvey, C. F. and Freeman, M. (2001). Regulated intracellular ligand transport and proteolysis control EGF signal activation in Drosophila. *Cell* **107**, 161-171.

Li, B., Gordon, G. M., Du, C. H., Xu, J. and Du, W. (2010). Specific killing of Rb mutant cancer cells by inactivating TSC2. *Cancer Cell* **17**, 469-480.

Lloyd, T. E., Atkinson, R., Wu, M. N., Zhou, Y., Pennetta, G. and Bellen, H. J. (2002). Hrs regulates endosome membrane invagination and tyrosine kinase receptor signaling in Drosophila. *Cell* **108**, 261-269.

Miura, G. I., Buglino, J., Alvarado, D., Lemmon, M. A., Resh, M. D. and Treisman, J. E. (2006). Palmitoylation of the EGFR ligand Spitz by Rasp increases Spitz activity by restricting its diffusion. *Dev. Cell* **10**, 167-176.

Miura, G. I., Roignant, J.-Y., Wassef, M. and Treisman, J. E. (2008). Myopic acts in the endocytic pathway to enhance signaling by the Drosophila EGF receptor. *Development* **135**, 1913-1922.

Moon, N.-S., Frolov, M. V., Kwon, E.-J., Di Stefano, L., Dimova, D. K., Morris, E. J., Taylor-Harding, B., White, K. and Dyson, N. J. (2005). Drosophila E2F1 has context-specific pro- and antiapoptotic properties during development. *Dev. Cell* **9**, 463-475.

Morris, E. J. and Dyson, N. J. (2001). Retinoblastoma protein partners. *Adv. Cancer Res.* **82**, 1-54.

Neuman-Silberberg, F. S. and Schüpbach, T. (1993). The Drosophila dorsoventral patterning gene gurken produces a dorsally localized RNA and encodes a TGF alpha-like protein. *Cell* **75**, 165-174.
Reich, A. and Shilo, B.-Z. (2002). Keren, a new ligand of the Drosophila epidermal growth factor receptor, undergoes two modes of cleavage. *EMBO J.* **21**, 4287-4296.
Royzman, I., Whittaker, A. J. and Orr-Weaver, T. L. (1997). Mutations in *Drosophila DP* and *E2F* distinguish G1-S progression from an associated transcriptional program. *Genes Dev.* **11**, 1999-2011.
Rutledge, B. J., Zhang, K., Bier, E., Jan, Y. N. and Perrimon, N. (1992). The Drosophila spitz gene encodes a putative EGF-like growth factor involved in dorsal-ventral axis formation and neurogenesis. *Genes Dev.* **6**, 1503-1517.
Ryoo, H. D., Gorenc, T. and Steller, H. (2004). Apoptotic cells can induce compensatory cell proliferation through the JNK and the Wingless signaling pathways. *Dev. Cell* **7**, 491-501.
Schnepp, B., Grumbling, G., Donaldson, T. and Simcox, A. (1996). Vein is a novel component in the Drosophila epidermal growth factor receptor pathway with similarity to the neuregulins. *Genes Dev.* **10**, 2302-2313.
Schweitzer, R., Shaharabany, M., Seger, R. and Shilo, B. Z. (1995). Secreted Spitz triggers the DER signaling pathway and is a limiting component in embryonic ventral ectoderm determination. *Genes Dev.* **9**, 1518-1529.
Steele, L., Sukhanova, M. J., Xu, J., Gordon, G. M., Huang, Y., Yu, L. and Du, W. (2009). Retinoblastoma family protein promotes normal R8-photoreceptor differentiation in the absence of rhinoceros by inhibiting dE2F1 activity. *Dev. Biol.* **335**, 228-236.
Steinhauer, J., Liu, H. H., Miller, E. and Treisman, J. E. (2013). Trafficking of the EGFR ligand Spitz regulates its signaling activity in polarized tissues. *J. Cell Sci.* **126**, 4469-4478.
Stevaux, O., Dimova, D. K., Ji, J.-Y., Moon, N. S., Frolov, M. V. and Dyson, N. J. (2005). Retinoblastoma family 2 is required in vivo for the tissue-specific repression of dE2F2 target genes. *Cell Cycle* **4**, 1272-1280.
Sturtevant, M. A., Roark, M., O'Neill, J. W., Biehs, B., Colley, N. and Bier, E. (1996). The Drosophila rhomboid protein is concentrated in patches at the apical cell surface. *Dev. Biol.* **174**, 298-309.
Sukhanova, M. J., Steele, L. J., Zhang, T., Gordon, G. M. and Du, W. (2011). RBF and Rno promote photoreceptor differentiation onset through modulating EGFR signaling in the Drosophila developing eye. *Dev. Biol.* **359**, 190-198.
Sun, Y., Jan, L. Y. and Jan, Y. N. (1998). Transcriptional regulation of atonal during development of the Drosophila peripheral nervous system. *Development* **125**, 3731-3740.
Tanaka-Matakatsu, M. and Du, W. (2008). Direct control of the proneural gene atonal by retinal determination factors during Drosophila eye development. *Dev. Biol.* **313**, 787-801.
Tanaka-Matakatsu, M., Xu, J., Cheng, L. and Du, W. (2009). Regulation of apoptosis of rbf mutant cells during Drosophila development. *Dev. Biol.* **326**, 347-356.
Tanaka-Matakatsu, M., Miller, J., Borger, D., Tang, W.-J. and Du, W. (2014). Daughterless homodimer synergizes with Eyeless to induce Atonal expression and retinal neuron differentiation. *Dev. Biol.* **392**, 256-265.
Tanaka-Matakatsu, M., Miller, J. and Du, W. (2015). The homeodomain of Eyeless regulates cell growth and antagonizes the paired domain-dependent retinal differentiation function. *Protein Cell* **6**, 68-78.
Treisman, J. E. (2013). Retinal differentiation in Drosophila. *Wiley Interdiscip. Rev. Dev. Biol.* **2**, 545-557.
Trimarchi, J. M. and Lees, J. A. (2002). Sibling rivalry in the E2F family. *Nat. Rev. Mol. Cell Biol.* **3**, 11-20.
Tsruya, R., Schlesinger, A., Reich, A., Gabay, L., Sapir, A. and Shilo, B.-Z. (2002). Intracellular trafficking by Star regulates cleavage of the Drosophila EGF receptor ligand Spitz. *Genes Dev.* **16**, 222-234.
Tsruya, R., Wojtalla, A., Carmon, S., Yogev, S., Reich, A., Bibi, E., Merdes, G., Schejter, E. and Shilo, B.-Z. (2007). Rhomboid cleaves Star to regulate the levels of secreted Spitz. *EMBO J.* **26**, 1211-1220.
Urban, S., Lee, J. R. and Freeman, M. (2001). Drosophila rhomboid-1 defines a family of putative intramembrane serine proteases. *Cell* **107**, 173-182.
van den Heuvel, S. and Dyson, N. J. (2008). Conserved functions of the pRB and E2F families. *Nat. Rev. Mol. Cell Biol.* **9**, 713-724.
Wessells, R. J., Grumbling, G., Donaldson, T., Wang, S.-H. and Simcox, A. (1999). Tissue-specific regulation of vein/EGF receptor signaling in Drosophila. *Dev. Biol.* **216**, 243-259.
Williams, R. L. and Urbé, S. (2007). The emerging shape of the ESCRT machinery. *Nat. Rev. Mol. Cell Biol.* **8**, 355-368.
Yogev, S., Schejter, E. D. and Shilo, B.-Z. (2010). Polarized secretion of Drosophila EGFR ligand from photoreceptor neurons is controlled by ER localization of the ligand-processing machinery. *PLoS Biol.* **8**, e1000505.
Zhang, T. and Du, W. (2015). Groucho restricts rhomboid expression and couples EGFR activation with R8 selection during Drosophila photoreceptor differentiation. *Dev. Biol.* **407**, 246-255.
Zhang, T., Ranade, S., Cai, C. Q., Clouser, C. and Pignoni, F. (2006). Direct control of neurogenesis by selector factors in the fly eye: regulation of atonal by Ey and So. *Development* **133**, 4881-4889.
Zhang, T., Liao, Y., Hsu, F.-N., Zhang, R., Searle, J. S., Pei, X., Li, X., Ryoo, H. D., Ji, J.-Y. and Du, W. (2014). Hyperactivated Wnt signaling induces synthetic lethal interaction with Rb inactivation by elevating TORC1 activities. *PLoS Genet.* **10**, e1004357.

SUPPLEMENTAL MATERIALS

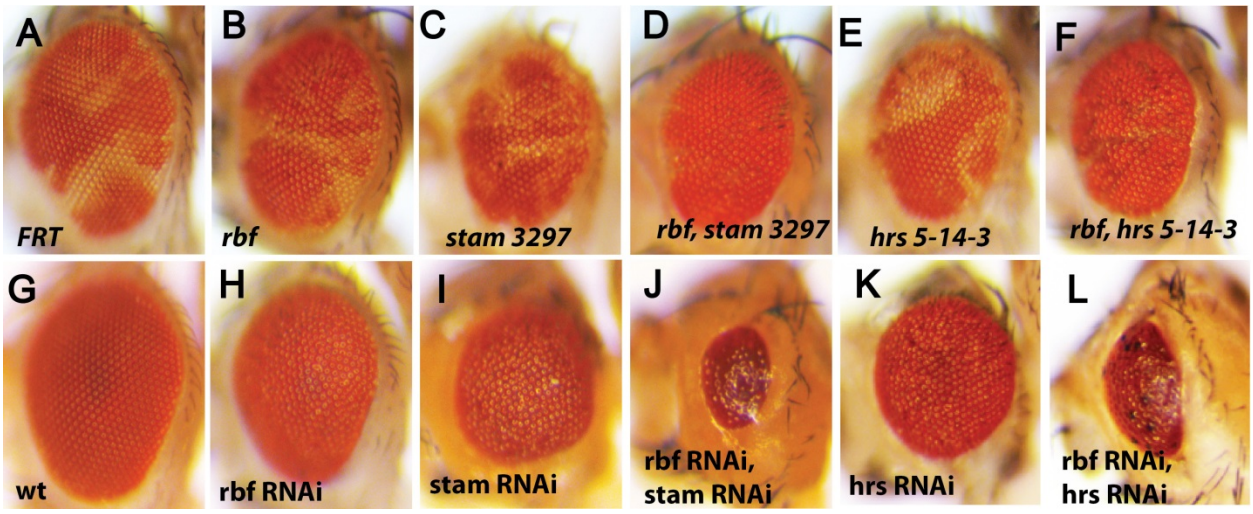

Figure S1. Inactivation of *rbf* with additional alleles of *stam* or *hrs* or using RNAi also causes the loss of double mutant tissues in adult eyes. (A-H) Representative pictures of adult eyes with clones of WT control (A), *rbf*, *stam*, *hrs* single- or double-mutant clones (B-F) are shown. (G-L) Pictures of adult eyes with single or double RNAi of rbf, stam, and hrs are shown. Inactivation of *rbf* with either *stam* or *hrs* led to the development of much smaller eyes.

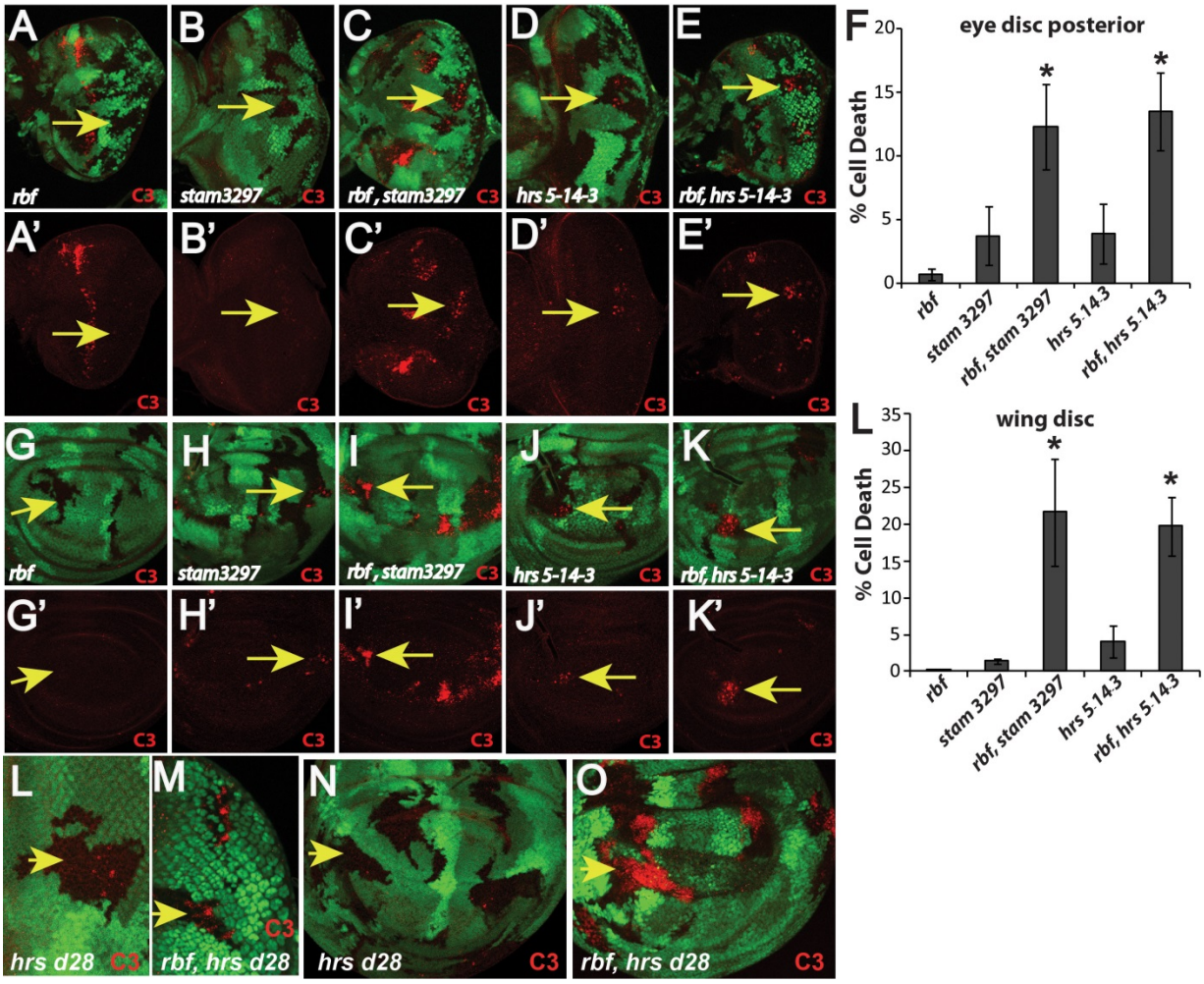

Figure S2. Inactivation of *rbf* with additional alleles of *stam* or *hrs* also induces synergistic cell death in the posterior of eye discs and in wing discs. Levels of apoptosis in 3rd instar eye discs (A-E', L-M) or wing discs (G-K', N-O) with *rbf*, *stam*, or *hrs* single or double mutant clones are shown. Specific stam and hrs alleles are indicated on each panel and mutant clones are marked by the lack of GFP and apoptosis detected by C3 staining. The level of apoptosis in mutant clones located in the posterior of eye discs and wing discs are quantified and the average and standard deviation are shown in (F) and (L), respectively ($N \geqslant 6$ for each genotype). Asterisks indicates statistically significant difference ($p<0.0005$) between double and each of the single mutant clones.

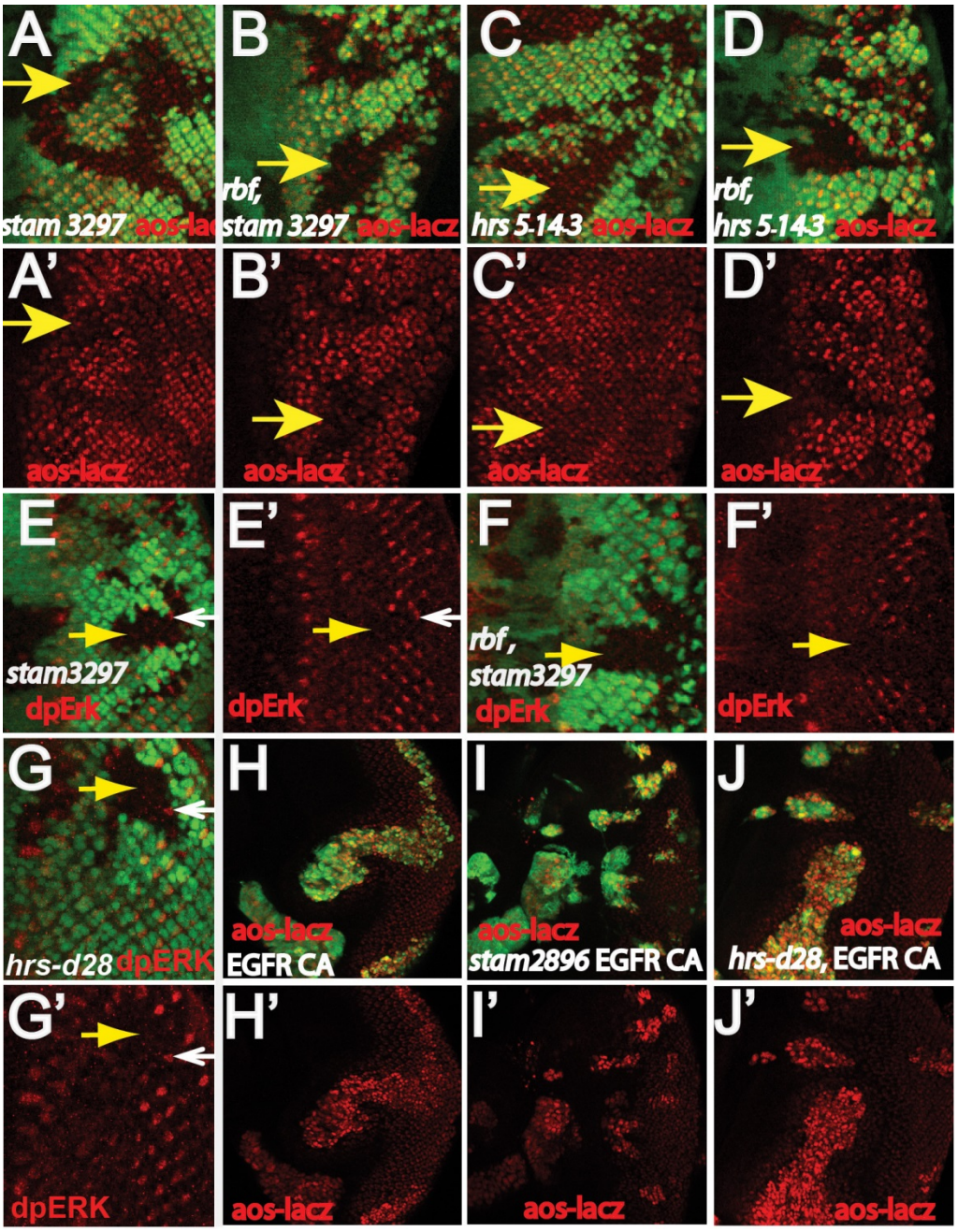

Figure S3. Additional alleles of *stam* and *hrs* also decrease EGFR signaling upstream of activated EGFR. (A-D) The effects of *stam*^{3297} (A-B) and *hrs*$^{5\text{-}14\text{-}3}$ (C-D) single mutant clones or double mutant clones with *rbf* (B and D) on aos-lacZ levels in posterior eye discs are shown. (E-G) *stam*^{3297}, *hrs*^{d28}, single- and *rbf stam*^{3297} double-mutant clones on MAP kinase activation in posterior eye discs are shown. The level of MAP kinase activation was detected by dpERK staining in red. Mutant clones are marked by the lack of GFP. Yellow arrows point to mutant clones in the posterior of eye discs. White arrows point to some of the mutant cells at the clone

boarder with high dpERK levels. (H-J) Null alleles of *stam* or *hrs* do not block activated EGFR-induced aos-lacZ. The EGFR signaling target aos-lacZ was strongly induced in eye discs by expressing activated EGFR in the following MARCM clones: WT (H), *stam* null allele $stam^{2896}$ (I), or *hrs* null allele hrs^{D28} (J). MARCM clones are marked by GFP expression.

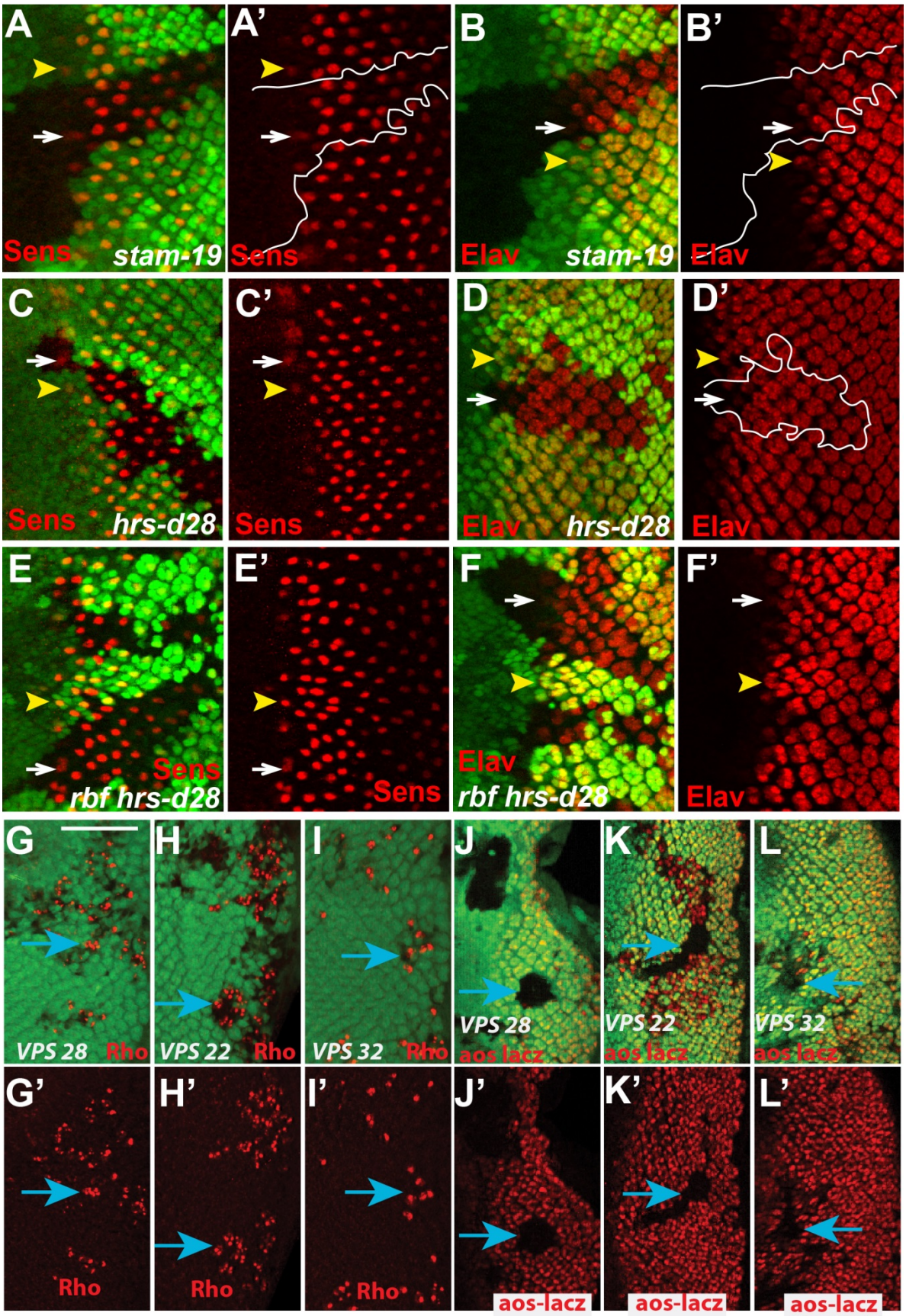

Journal of Cell Science • Supplementary information

Figure S4. The effects of stam or hrs mutation on photoreceptor differentiation and the effects of other ESCRT complexes on rhomboid and EGFR signaling. (A-F) Mutations of *stam* or *hrs* do not significantly affect R8 differentiation but delay the differentiation of additional photoreceptors. (A-B) $stam^{19}$ mutation did not significantly affect the differentiation of R8 photoreceptors as determined by R8 marker Senseless (Sens) (A) but slightly delayed the differentiation of additional photoreceptors (B). (C-F) hrs^{d28} null mutant (C-D) or hrs^{d28} *rbf* double mutants (E-F) also displayed little effect on R8 differentiation as shown by Sens expression (C and E) but exhibited more significant delay in the differentiation of additional photoreceptors as shown by significantly delayed induction of Elav (D and F). Yellow arrowheads point to the regions where Sens or Elav expression is initiated in WT eye discs and white arrows point to the corresponding regions in mutant clones. (G-L) Mutations of other ESCRT complexes also affect Rhomboid endosomal trafficking and reduce expression of the EGFR signaling reporter aos-lacZ. Mutations in components of ESCRT-I (*VPS 28*, G and J), ESCRT-II (*VPS 22,* H and K), or ESCRT-III (*VPS 32,* I and L) affect Rhomboid endosomal trafficking (G-I) and expression of the EGFR signaling reporter aos-lacZ (J-L). Scale bar, 50 μm.

Table S1. Genotypes used in this study.

Fig. 1
w, eyFLP (or HsFLP)/Y; Ubi-GFP, FRT40A/FRT40A
$rbf^{15a\Delta}$,w, eyFLP (or HsFLP)/Y; RBF-G3, Ubi-GFP, FRT40A/FRT40A
w, eyFLP (or HsFLP)/Y; Ubi-GFP, FRT40A/ *stam* (or *hrs*), FRT40A
$rbf^{15a\Delta}$,w, eyFLP (or HsFLP)/Y; RBF-G3, Ubi-GFP, FRT40A/*stam* (or *hrs*) FRT40A
Fig. 2
$rbf^{15a\Delta}$,w, eyFLP (or HsFLP)/Y; RBF-G3, Ubi-GFP, FRT40A/FRT40A
w, eyFLP (or HsFLP)/Y; Ubi-GFP, FRT40A/ *stam* (or *hrs*), FRT40A
$rbf^{15a\Delta}$,w, eyFLP (or HsFLP)/Y; RBF-G3, Ubi-GFP, FRT40A/*stam* (or *hrs*) FRT40A
$rbf^{15a\Delta}$,w, eyFLP /Y; RBF-G3, Ubi-GFP, FRT40A/$stam^{19}$,FRT40A; hid^{138}/hid^{138}
$rbf^{15a\Delta}$,w, eyFLP /Y; RBF-G3, Ubi-GFP, FRT40A/$stam^{19}$,FRT40A; $de2f1^{i2}/de2f1^{rm729}$
Fig. 3
w, eyFLP (or HsFLP)/Y; Ubi-GFP, FRT40A/FRT40A
$rbf^{15a\Delta}$,w, eyFLP (or HsFLP)/Y; RBF-G3, Ubi-GFP, FRT40A/FRT40A

w, eyFLP (or HsFLP)/Y; Ubi-GFP, FRT40A/ *stam* (or *hrs*), FRT40A

rbf$^{15a\Delta}$,w, eyFLP (or HsFLP)/Y; RBF-G3, Ubi-GFP, FRT40A/*stam* (or *hrs*) FRT40A

w, HsFLP/Y; Ubi-GFP, FRT40A/FRT40A; aos-lacz

rbf$^{15a\Delta}$,w, eyFLP /Y; RBF-G3, Ubi-GFP, FRT40A/FRT40A; aos-lacz

w, eyFLP (or HsFLP)/Y; Ubi-GFP, FRT40A/ *stam* (or *hrs*), FRT40A; aos-lacz (or rho-lacz)

rbf$^{15a\Delta}$,w, eyFLP /Y; RBF-G3, Ubi-GFP, FRT40A/*stam* (or *hrs*) FRT40A; aos-lacz

w, HsFLP/Y; tub-Gal80, FRT40A/*stam*^{19}, FRT40A; Act > y >Gal4, UAS-GFP / aos-lacz

Fig. 4

rbf$^{15a\Delta}$,w, eyFLP /Y; RBF-G3, tub-Gal80, FRT40A/FRT40A; Act > y >Gal4, UAS-GFP/+ (or UAS-Rho)

rbf$^{15a\Delta}$,w, eyFLP /Y; RBF-G3, tub-Gal80, FRT40A/*stam*^{19}, FRT40A; Act > y >Gal4, UAS-GFP / + (or UAS-ras^{v12}, or UAS-EGFR^{CA}, or UAS-rho1)

rbf$^{15a\Delta}$,w, hsFLP /Y; RBF-G3, tub-Gal80, FRT40A/*stam*^{19},FRT40A; Act > y >Gal4, UAS-GFP / UAS-sSpi

Fig. 5

w, HsFLP/Y; tub-Gal80, FRT40A/FRT40A; Act > y >Gal4, UAS-GFP /UAS-rho1, aos-lacz (or UAS-EGFR^{CA}, aos-lacz; or UAS-sSpi, aos-lacz)

w, HsFLP/Y; tub-Gal80, FRT40A/*stam*^{19}, FRT40A; Act > y >Gal4, UAS-GFP /UAS-rho1, aos-lacz (or UAS-EGFR^{CA}, aos-lacz; or UAS-sSpi, aos-lacz)

w, HsFLP/Y; tub-Gal80, FRT40A/FRT40A; Act > y >Gal4, UAS-GFP /UAS-rho1 (or UAS-EGFR^{CA})

w, HsFLP/Y; tub-Gal80, FRT40A/*stam*^{19}, FRT40A; Act > y >Gal4, UAS-GFP/UAS-rho1 (or UAS-EGFR^{CA})

Fig. 6

w, HsFLP/Y; Arm-lacz, FRT40A/FRT40A; GMR-Gal4/Rab5-YFP (or Rab7-YFP)

w, HsFLP/Y; Arm-lacz, FRT40A/*stam*^{19}, FRT40A; GMR-Gal4/Rab5-YFP (or Rab7-YFP)

w, HsFLP/UAS-mSpi-GFP; Arm-lacz, FRT40A/*stam*^{19}, FRT40A, Sca-Gal4

w, eyFLP (or HsFLP)/Y; Ubi-GFP, FRT40A/FRT40A

w, eyFLP (or HsFLP)/Y; Ubi-GFP, FRT40A/ *stam* (or *hrs*), FRT40A

w, eyFLP (or HsFLP)/Y; Ubi-GFP, FRT40A/ *stam* (or *hrs*), FRT40A; rho-lacz)

Fig. S1

eyFlp, Act>CD2>Gal4; UAS-Rbf RNAi; + (or UAS-stam RNAi, or UAS-hrs RNAi)

eyFlp, Act>CD2>Gal4; UAS-stam RNAi (or UAS-hrs RNAi)

w, eyFLP (or HsFLP)/Y; Ubi-GFP, FRT40A/FRT40A

rbf$^{15a\Delta}$,w, eyFLP (or HsFLP)/Y; RBF-G3, Ubi-GFP, FRT40A/FRT40A

w, eyFLP (or HsFLP)/Y; Ubi-GFP, FRT40A/ *stam* (or *hrs*), FRT40A

rbf$^{15a\Delta}$,w, eyFLP /Y; RBF-G3, Ubi-GFP, FRT40A/*stam* (or *hrs*) FRT40A

Fig. S2

rbf$^{15a\Delta}$,w, eyFLP (or HsFLP)/Y; RBF-G3, Ubi-GFP, FRT40A/FRT40A

w, eyFLP (or HsFLP)/Y; Ubi-GFP, FRT40A/ *stam* (or *hrs*), FRT40A

rbf$^{15a\Delta}$,w, eyFLP (or HsFLP)/Y; RBF-G3, Ubi-GFP, FRT40A/*stam* (or *hrs*) FRT40A

Fig. S3

w, eyFLP /Y; Ubi-GFP, FRT40A/ *stam* (or *hrs*), FRT40A; aos-lacz

rbf$^{15a\Delta}$,w, eyFLP /Y; RBF-G3, Ubi-GFP, FRT40A/*stam* (or *hrs*), FRT40A; aos-lacz

w, eyFLP/Y; Ubi-GFP, FRT40A/ *stam* ^{3297}, FRT40A

rbf$^{15a\Delta}$,w, eyFLP /Y; RBF-G3, Ubi-GFP, FRT40A/*stam* ^{3297},FRT40A

w, HsFLP/Y; tub-Gal80, FRT40A/ *hrs* ^{d28} (or *stam* ^{2896}), FRT40A; Act > y >Gal4, UAS-GFP / UAS-EGFR^{CA}, aos-lacz

Fig. S4

w, HsFLP/Y; Ubi-GFP, FRT40A/ *stam*^{19} (or *hrs* ^{d28}), FRT40A

rbf$^{15a\Delta}$,w, HsFLP/Y; RBF-G3, Ubi-GFP, FRT40A / *hrs*^{d28} FRT40A

w, HsFLP/Y; FRT82B, Ubi-GFP/ aos-lacz ,FRT82B, *vps22*

w, HsFLP/Y; FRT82B, Ubi-GFP/ FRT82B, *vps22*

w, HsFLP/Y; FRT42D, Ubi-GFP/ FRT42D, *vps28*; + (or aos-lacz)

w, HsFLP/Y; FRT42D, Ubi-GFP/ FRT42D, *vps32*; + (or aos-lacz)

Journal of Cell Science • Supplementary information